Contents lists available at ScienceDirect

European Journal of Mechanics B/Fluids

On the role of unsteady forcing of tracer gradient in local stirring

M. Gonzalez*, P. Paranthoën

CNRS, UMR 6614/CORIA, Site universitaire du Madrillet, 76801 Saint-Etienne du Rouvray, France

ARTICLE INFO

ABSTRACT

Local stirring properties in two basic mixing flows – namely, the blinking vortex and the sine flow – are studied through the tracer gradient approach. The velocity gradient tensor and related quantities such as the strain persistence parameter are derived from the analytical velocity fields. Numerical Lagrangian tracking of the gradient of a tracer shows how local stirring is affected by forcing experienced through strain persistence. In both flows Lagrangian variations of strain persistence occuring on a time scale shorter than the response time scale of the tracer gradient lead the latter to align close to the direction determined by the mean strain persistence. It is the special alternating behaviour of strain persistence resulting from flow operation that makes this direction coincide with the local compressional strain direction for both the sine flow and the clockwise/counterclockwise blinking vortex. The rise of the tracer gradient and thus local stirring are in turn promoted by this statistical alignment.

© 2009 Elsevier Masson SAS. All rights reserved.

1. Introduction

Mixing phenomena in fluid flows are far from being fully explained, despite significant progress in the study of scalar transport by laminar or turbulent flows. In a number of cases questions such as "which stirring gives the most efficient mixing?" or "how long does it take to reach a given mixed state?" remain unanswered. Actually, there is still an intense need of basic studies devoted to mixing phenomena, more especially as many industrial processes use mixing flows. In chemical processes, for instance, reactions may take place in a poorly mixed medium, well before homogenization is achieved, thus causing damage of product quality or bringing about an excess of pollution. Developing processes which ensure energy sparing, improvement of safety and productive capacity together with low pollutant release therefore needs designing devices in which mixing would be well understood and controlled.

As is well established, mixing in fluid flows is essentially a matter of stirring and molecular diffusion. Stirring makes fluid-element pairs separate which is also seen as stretching of material lines or surfaces. It is taken for granted that stretching promotes mixing. Indeed the higher the stretching, the larger the contact area and the smaller the distance between fluid portions to be mixed.

Hence the hastening of molecular diffusion and homogenization of the mixture. In addition, "good mixing" often implies a uniform distribution of stretching rate within the flow.

Understanding the advective part of mixing during which the mechanical action of fluid flow produces small scales of the scalar field – heat, contaminant …– through "cascade phenomena" without significant influence of molecular diffusion is a big issue of turbulent mixing, especially in large-Péclet-number flows [1]. The passive scalar cascade and the way in which it may be connected to mixing studies have been investigated through the statistical approach [2,3]. The study of advective mechanisms of mixing is also relevant to chaotic mixing [4,5]. In this regard, different approaches have been used, namely those based on Lyapunov exponents [4], on the concept of effective diffusivity [6] or on geometrical properties of flows defined through stable and unstable manifolds [4]. The latter geometrical approach, in particular, provides a thorough knowledge of mixing properties of two- and three-dimensional unsteady flows. Efficiency of mixing, for instance, may be qualitatively diagnosed through the detection of barriers to transport.

The approach based on the evolution of the gradient of a passive scalar – or tracer – transported by the flow arises from a natural idea, for cascade mechanisms result in production of large gradients and micromixing efficiency is measured by the mean dissipation rate of tracer fluctuations, a quantity proportional to the variance of the tracer gradient [3]. The rise of the local, instantaneous gradient of a non-diffusive tracer is equivalent to the stretching of fluid elements and both mechanisms have been used to investigate turbulent [7,8] as well as chaotic mixing [9,10]. It is

* Corresponding author. Tel.: +33 2 32 95 37 05; fax: +33 2 32 91 04 85.
 E-mail address: Michel.Gonzalez@coria.fr (M. Gonzalez).

also worth mentioning that properties of Lyapunov vectors and exponents can be understood through the tracer gradient dynamics [11]. In addition, by providing quantitative insight into local stirring properties, the tracer gradient approach is to a great extent complementary to the geometrical approach. The tracer gradient properties are even basically connected to the structure of mixing patterns in that the gradient direction and magnitude respectively correspond to the striation orientation and thickness – fine structures meaning large gradients –. Moreover, as concentration contours tend to align with manifolds in chaotic regions and almost homogeneous tracer patches lie in islands, mixing patterns are tightly linked to coherent structures in tracer trajectories.

Production of the norm of a tracer gradient – which in turn promotes mixing through the resulting accelerated molecular diffusion – rests on both strain intensity and gradient orientation with respect to strain principal axes. Orientation of tracer gradient in the strain basis stems from the combination of strain, vorticity, strain basis rotation and molecular diffusion [12]; strain basis rotation itself depends on strain, vorticity, pressure and viscous effects [12] and so do the strain eigenvalues. These established facts suggest the intricacy of the mechanisms underlying the mixing process. In three-dimensional flows analytical approaches are unfeasible unless simplifying hypotheses on the dynamic field are made [13]. Assuming the flow to be two-dimensional and neglecting molecular diffusion make the problem somewhat simpler and even analytically tractable in some special cases [7].

Even so, mixing problems have most often to be addressed in unsteady conditions. Actually, non-stationary aspects of the mixing process are essential in the turbulent as well as in the chaotic regimes. In the view of the tracer gradient approach, then, one has to examine mixing properties of fluid flows through the dynamics of the tracer gradient, namely through its response to varying mechanical actions or forcing. The dynamics of scalar gradient alignment, for instance, has been addressed in some previous studies [12,14,15]. Recently, it has also been shown that in two-dimensional flow – more specifically in the laminar Bénard – von Kármán street [16,17] – forcing through Lagrangian variations of strain persistence may deeply affect tracer gradient behaviour in terms of alignment properties and norm growth rate. In particular, local orientation of the tracer gradient appears to be strongly dependent on whether or not the gradient responds to this kind of forcing. Further investigation needs addressing some remaining questions, more especially: i) is the latter behaviour observed in various flows or is it restricted to some class of flows? and ii) how are local stirring properties of the flow determined by this tracer gradient dynamics?

The present study deals with these questions by analysing the kinematics of the tracer gradient in two model mixing flows. We more specifically focus on the conditions in which local stirring may be enhanced by unsteady forcing. This is done in Section 3 in which the tracer gradient behaviour is investigated numerically starting from the analytical definition of the flow. Theoretical bases on the dynamics of the gradient of a non-diffusive tracer in two-dimensional flows are given in Section 2. Section 4 is devoted to conclusion.

2. Stirring properties considered through the behaviour of the tracer gradient

We address the mechanisms of local stirring, that is, the advective part of mixing during which fine structures form in the mixing pattern. Since small-scale structures such as thin filaments imply high gradients, this process also finds expression in enhancement of the gradient of a non-diffusive scalar or tracer convected by the flow. The analysis is relevant to the mixing of

high-Schmidt number quantities as well as to the large-Péclet-number regime in which a significant stage of the mixing process is filled by production of small scales by stretching before diffusive homogenization takes place.

In two-dimensional flows, then, the behaviour of the tracer gradient can be rigorously analysed from the velocity gradient properties [7,15]. In this approach the tracer gradient, $\boldsymbol{G}$, is determined through its orientation and norm which are given by Eqs. (1) and (2) [7]:

$$\frac{d\zeta}{dt} = \sigma(r - \cos\zeta), \tag{1}$$

$$\frac{2}{|\boldsymbol{G}|}\frac{d|\boldsymbol{G}|}{dt} = -\sigma\sin\zeta, \tag{2}$$

in which $\boldsymbol{G} = |\boldsymbol{G}|(\cos\theta, \sin\theta)$ and $\zeta = 2(\theta + \Phi)$ gives the gradient orientation in the local strain basis (Fig. 1). Orientation of strain principal axes, Φ, is defined by $\tan(2\Phi) = \sigma_n/\sigma_s$ where $\sigma_n = \partial u/\partial x - \partial v/\partial y$ and $\sigma_s = \partial v/\partial x + \partial u/\partial y$ respectively denote the normal and shear components of strain; u and v are the velocity components. Strain rate, σ, is given by $\sigma = (\sigma_n^2 + \sigma_s^2)^{1/2}$. In Eq. (1) r is the strain persistence parameter which measures the respective effects of effective rotation – vorticity plus rotation rate of strain principal axes – and strain and is defined as:

$$r = \frac{\omega + 2d\Phi/dt}{\sigma}, \tag{3}$$

where $\omega = \partial v/\partial x - \partial u/\partial y$ is vorticity.

As shown by Lapeyre et al. [7], the strain persistence parameter, r, defines a criterion to partition the flow in regions with different stirring properties. In strain-dominated regions, $r^2 < 1$, the tracer
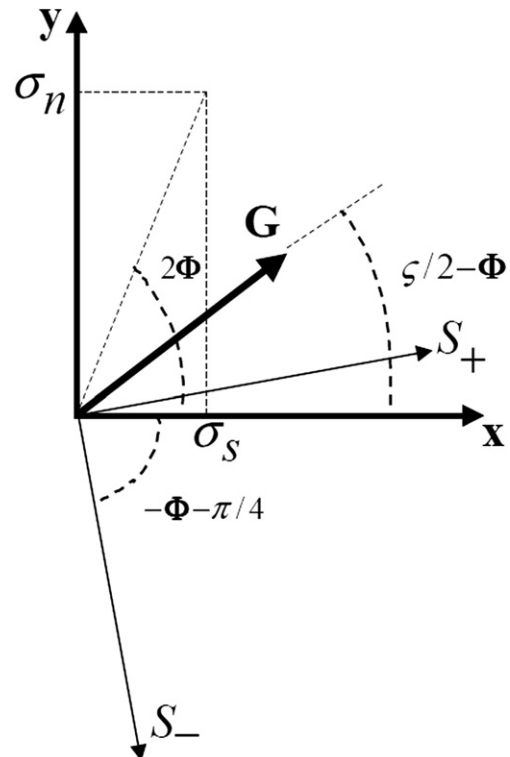

Fig. 1. Schematic of reference frames; S_- and S_+ respectively stand for compressional and extensional strain axes.

gradient tends to align with a local equilibrium orientation given by $\zeta_{eq} = -\arccos(r)$; the gradient norm grows exponentially at the rate $\sigma(1-r^2)^{1/2}/2$ in terms of the strain-normalised time, $\tau = \int_0^t \sigma(t')\mathrm{d}t'$. The maximum growth rate is reached for $r = 0$, in the pure hyperbolic regime, if the equilibrium orientation coincides with the strain compressional direction given by $\zeta_c = -\pi/2$. In rotation-dominated regions, $r^2 > 1$, there is no equilibrium orientation for the tracer gradient; instead, the gradient has a most probable orientation, namely $\zeta_{prob} = [1 - sign(r)]\pi/2$ and its norm does not grow. Balance between strain and effective rotation, $r^2 = 1$, drives the tracer gradient to align with a bisector of strain principal axes defined by $\zeta_s = 0$ or $\zeta_s = -\pi$ and its norm grows linearly with τ. This partition may depart from the one given by the widely used Okubo–Weiss criterion [18,19]; because r includes the strain basis rotation rate – while in the Okubo–Weiss criterion the rotation term is limited to vorticity –, the criterion based on strain persistence is more general and has been shown to give a better estimate of local stirring properties [7]. Note that accounting for rotation rate of strain principal axes had been proposed by Dresselhaus and Tabor [20] and that a strain persistence parameter based on effective rotation had also been defined by Tabor and Klapper [21].

A key assumption underlying the analysis by Lapeyre et al. [7] is that r varies "slowly" along Lagrangian trajectories. It has been more specifically shown [16,17] that this approach remains valid as long as the response time scale of the tracer gradient – which, as suggested by Eq. (1), is of the order of $1/\sigma$ – is short enough compared to the time scale of the Lagrangian variations of r which force the gradient through its orientation, ζ. Indeed perfect response of the tracer gradient brings about preferential alignment with a direction determined by the local value of strain persistence, r, in agreement with the analysis of Lapeyre et al. [7]. Poor response, by contrast, has been found to make the tracer gradient statistically align with an orientation given by the mean value of strain persistence, $\langle r \rangle$, which indicates whether the flow is, *on an average*, either strain- or effective-rotation dominated. Garcia et al. [16,17] have shown the existence of the latter regimes in a laminar Bénard – von Kármán street and checked corresponding alignment with either $\zeta_{\langle r \rangle} = -\arccos\langle r \rangle$ or $\zeta_{\langle r \rangle} = [1 - sign\langle r \rangle]\pi/2$. Interestingly, numerical simulations of two-dimensional turbulence [7] show preferential alignment of tracer gradient with the direction determined by the *local* value of strain persistence thus suggesting a possible essential feature of scalar gradient dynamics in turbulent flows. A condition especially relevant to stirring is defined by zero average strain persistence, $\langle r \rangle \simeq 0$; in this case, fast variations of r – as compared to the tracer gradient response – drives the gradient orientation to remain close to the local compressional direction for which the norm growth rate is maximum [17]. In order to assess further the connection of local stirring properties with the unsteady behaviour of the tracer gradient, we investigate two different basic mixing flows.

3. Local stirring and tracer gradient behaviour in two model mixing flows

3.1. Blinking vortex flow

We consider the mixing device based on the blinking vortex flow [22] regularized as proposed by Kin and Sakajo [23]. The system is made of two agitators, namely P_1 and P_2; their rotation is controlled in terms of direction and duration. It is assumed that the fluid motion starts as soon as one of the agitators begins to rotate and stops as soon as rotation is switched off. The velocity field resulting from rotation of one agitator P_i ($i = 1, 2$) is defined by analytical velocity components:

$$u_i = -\frac{\Gamma_i}{2\pi}\frac{y - q_i}{(x - p_i)^2 + (y - q_i)^2 + \delta^2}, \tag{4}$$

$$v_i = \frac{\Gamma_i}{2\pi}\frac{x - p_i}{(x - p_i)^2 + (y - q_i)^2 + \delta^2}, \tag{5}$$

where (p_i, q_i) defines the location of P_i in the (x, y) system of reference and Γ_i is the strength of the vortex blob generated by rotation of agitator P_i. The velocity field is regularized through parameter δ; with $\delta = 0$, the flow field would correspond to the one resulting from a vortex point in an incompressible, inviscid fluid which diverges for (x, y) tending to (p_i, q_i).

The conditions of the study are the same as those chosen by Kin and Sakajo [23]: $(p_1, q_1) = (-1/2, 0)$, $(p_2, q_2) = (1/2, 0)$ and $\Gamma_i = \pm 1$. Clockwise rotation corresponds to $\Gamma_i = -1$ and counterclockwise rotation to $\Gamma_i = 1$. The device is operated by switching the agitators on and off each one in its turn. During a basic operation P_1 rotates during a given time interval, T, then is switched off and P_2 rotates during the same time interval. A mixing operation consists of N basic operations. Rotation duration, T, is given by $T = 2\pi^2(\delta^2 + 1/4)$. The influence of δ has been checked by Kin and Sakajo [23]; in this study $\delta = 0.6$, a value they specifically used. Clockwise rotation of P_i is denoted by $n(i)$ and counterclockwise rotation by $p(i)$. We analyse two different mixing processes: the first one consists of N $p(1)p(2)$ forcing periods – both agitators rotate counterclockwise –, while in the second one the basic operations are of $p(1)n(2)$ type – P_1 and P_2 respectively rotate counterclockwise and clockwise –. Differences in stirring properties of $p(1)p(2)$ and $p(1)n(2)$ processes are scrutinized through the behaviour of the tracer gradient.

The approach needs the velocity gradient. The latter is easily derived from Eqs. (4) and (5) and used to analytically express strain components, vorticity and strain basis rotation rate:

$$\sigma_n = \frac{2\Gamma_i}{\pi}\frac{x'y'}{\rho^4}, \tag{6}$$

$$\sigma_s = -\frac{\Gamma_i}{\pi}\frac{x'^2 - y'^4}{\rho^4}, \tag{7}$$

$$\omega = \frac{\Gamma_i}{\pi}\frac{\delta^2}{\rho^4}, \tag{8}$$

$$2\frac{\mathrm{d}\Phi}{\mathrm{d}t} = -\frac{\Gamma_i}{\pi\rho^2}, \tag{9}$$

with $x' = x - p_i$, $y' = y - q_i$ and $\rho^2 = x'^2 + y'^2 + \delta^2$. The strain persistence parameter is derived from Eq. (3) and Eqs. (6)–(9):

$$r = -\frac{\Gamma_i}{|\Gamma_i|}. \tag{10}$$

This is a significant result which means that in the blinking vortex system the strain persistence parameter is constant all over the flow field during rotation of either P_1 or P_2. More precisely, $r = 1$ for clockwise rotation of P_i and $r = -1$ for counterclockwise rotation. These special values of r indicate that effective rotation – not just vorticity – and strain balance each other, a result already mentioned for the single point vortex [24]. Moreover, $p(1)p(2)$ and $p(1)n(2)$ processes respectively correspond to two different kinds of forcing of the tracer gradient through strain persistence; the former induces steady forcing ($r = -1$) of the tracer gradient orientation, while the latter results in unsteady forcing (r periodically takes values -1 and 1).
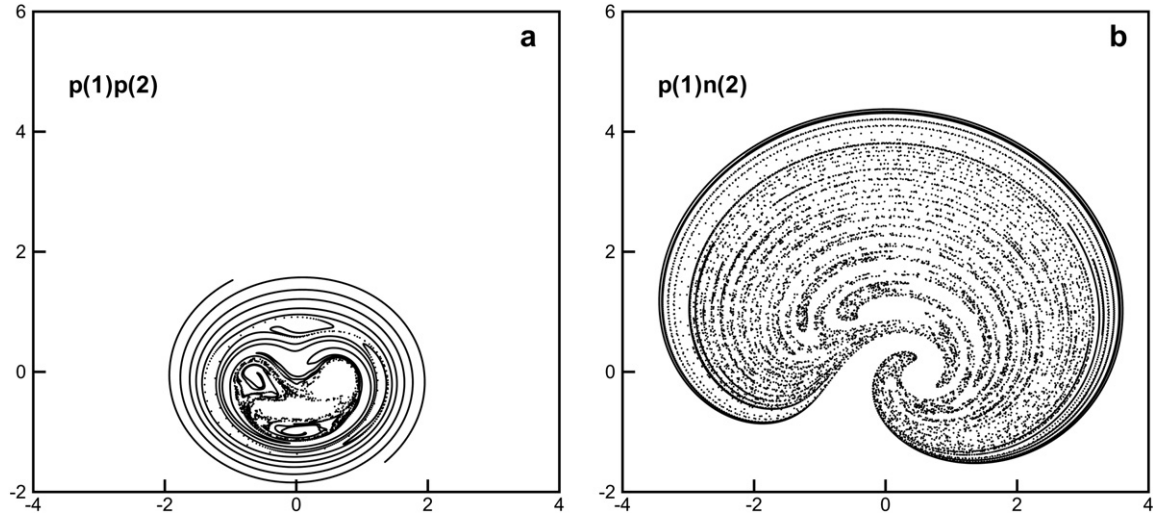
Fig. 2. Positions of 20 000 particles, initially located on line $[-2 \leq x \leq 2, y = 0]$, after 16 period times; (a) $p(1)p(2)$ process; (b) $p(1)n(2)$ process.

Fig. 2 displays the positions – computed using Eqs. (4) and (5) – of 20 000 particles, initially set on line $[-2 \leq x \leq 2, y = 0]$, after 16 period times, a test case already studied by Kin and Sakajo [23]. As suggested by the figure, $p(1)n(2)$ most likely spreads material out much better than $p(1)p(2)$ does which is confirmed in more details by Kin and Sakajo [23]. Actually, $p(1)p(2)$ accomodates unmixed regions, while $p(1)n(2)$ ensures chaotic conditions and thus better global mixing. From a practical point of view, local stirring properties of process $p(1)p(2)$ may therefore be a question of minor importance. All the same we consider $p(1)p(2)$ to clearly show the difference in stirring properties resulting from forcing via either steady – $p(1)p(2)$ – or unsteady – $p(1)n(2)$ – strain persistence. As shown in the following, $p(1)n(2)$ process is more efficient than $p(1)p(2)$ in this respect as well.

Lagrangian Eqs. (1) and (2) for the orientation and norm of the tracer gradient are numerically solved for both $p(1)p(2)$ and $p(1)n(2)$ processes. The integration time step is $\Delta t = 0.001\,T$ and the total number of forcing periods is $N = 16$. The differences between both processes are first illustrated by tracking the evolution of the

tracer gradient along the trajectory of a test particle initially located at $x(0) = -2$ and $y(0) = -1.3 \times 10^{-7}$. The trajectory is integrated using the velocity field given by Eqs. (4) and (5). The initial orientation of the gradient is $\zeta(0) = \pi/4$ and its initial norm, $|\mathbf{G}|(0) = 1$.

The normalised strain rate, $\sigma^* = \sigma/\sigma_m$, experienced by the tracer gradient along the Lagrangian trajectory of the test particle – where $\sigma_m = (\Gamma_i/4\pi\delta^2)^2$ is the maximum strain rate caused by the device – is displayed in Fig. 3. The respective evolutions in $p(1)p(2)$ and $p(1)n(2)$ processes are different, but the gradient undergoes, on an average, a comparable strain rate. The difference in the evolution of the tracer gradient orientation is more striking. As shown in Fig. 4, in the $p(1)p(2)$ process the steady value of strain persistence, $r = -1$, drives the tracer gradient to align with the bisector of strain principal axes defined by $\zeta_s = -\pi$, in agreement with the analysis of Lapeyre et al. [7]. During the $p(1)n(2)$ process, by contrast, the alternating behaviour of strain persistence, $r = \pm 1$, prevents alignment from constantly tending to either $\zeta_s = -\pi$ or $\zeta_s = 0$; the tracer gradient orientation remains close to the compressional direction given by $\zeta_c = -\pi/2$ which corresponds to alignment determined by
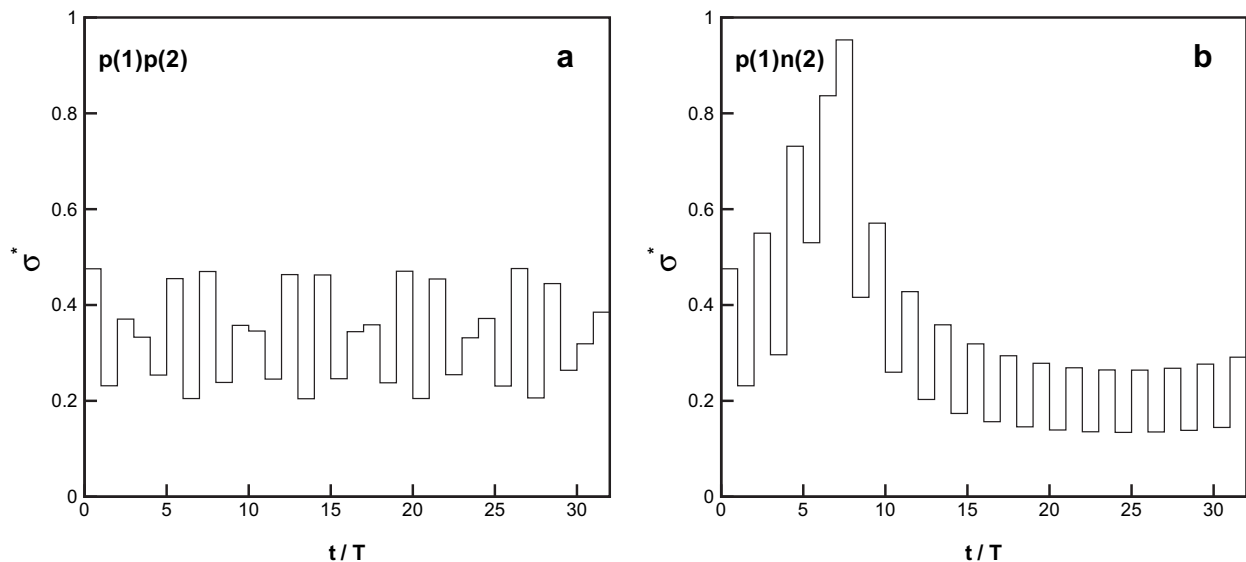

Fig. 3. Lagrangian evolution of strain rate for the test particle; (a) $p(1)p(2)$ process; (b) $p(1)n(2)$ process.
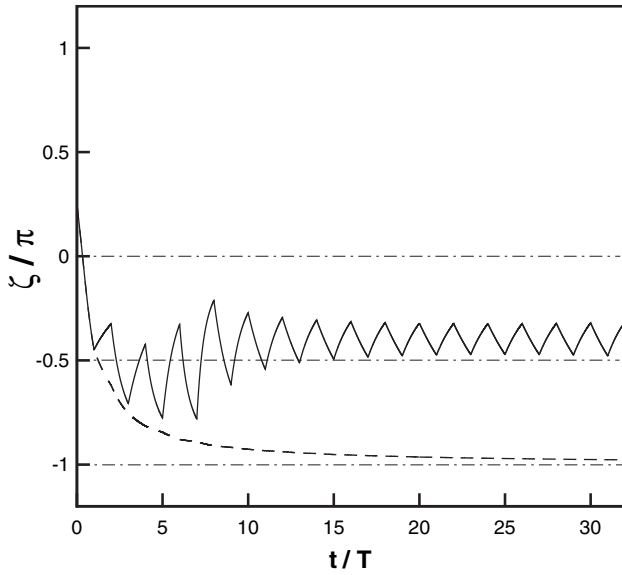
Fig. 4. Lagrangian evolution of tracer gradient orientation for the test particle; dashed line: $p(1)p(2)$ process; solid line: $p(1)n(2)$ process.

Fig. 6. Lagrangian evolution of tracer gradient norm for the test particle; dashed line: $p(1)p(2)$ process; solid line: $p(1)n(2)$ process.

the mean strain persistence, $\langle r \rangle = 0$ in the present case. Alignment of the tracer gradient has a big effect on the norm growth rate. As shown in Fig. 5, the normalised growth rate, $\eta^* = \eta/\eta_\mathrm{m}$ – with $\eta = -(\sigma \sin \zeta)/2$ and $\eta_\mathrm{m} = \sigma_\mathrm{m}/2$ –, tends to vanish along the Lagrangian trajectory in the $p(1)p(2)$ process, while it is sustained in the $p(1)n(2)$ process. As a result, the $p(1)n(2)$ process causes a much larger rise of the gradient norm (Fig. 6).

The behaviour pictured by the Lagrangian tracking of a single particle is confirmed by statistics computed on 60 501 particles initially located on a regular mesh over the spatial domain defined by $-4 \leq x \leq 4$ and $-6 \leq y \leq 6$. Particles are tracked all along 16 forcing periods of agitators P_1 and P_2. For each particle, the initial norm of the tracer gradient is unity and the initial gradient orientation is $\zeta(0) = 0$. It has been checked that initial orientation does not significantly affect the tracer gradient statistics.
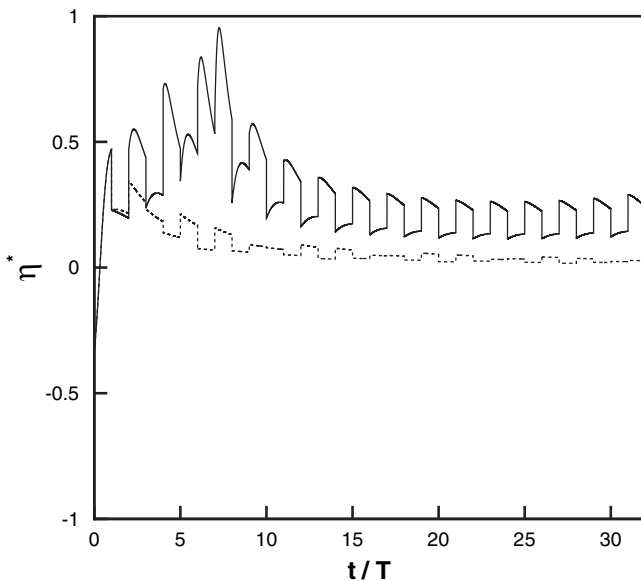
Fig. 7 displays the p.d.f of strain rate computed over all the Lagrangian trajectories. This p.d.f is the same for both $p(1)p(2)$ and $p(1)n(2)$ processes. Clearly, the most probable values of strain rate – in other words, the most probable values of the frequency of tracer gradient response – lie below the frequency, $1/T$, of the periodical forcing imposed by the alternating strain persistence in $p(1)n(2)$ process. In the latter case the tracer gradient thus does not keep up with strain persistence variations and, as shown in Fig. 8, statistically aligns with the direction defined by the mean strain persistence, $\langle r \rangle = 0$, – hence with the compressional direction, ζ_c – rather than with direction ζ_s corresponding to the instantaneous value, $r = \pm 1$. In the $p(1)p(2)$ process, by contrast, forcing resulting from the steady value of strain persistence drives the tracer gradient to align with ζ_s.

Fig. 5. Lagrangian evolution of tracer gradient norm growth rate for the test particle; dashed line: $p(1)p(2)$ process; solid line: $p(1)n(2)$ process.
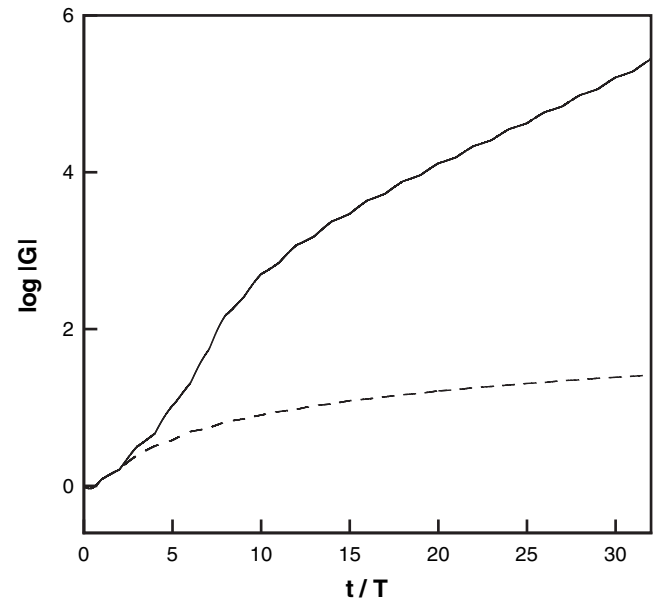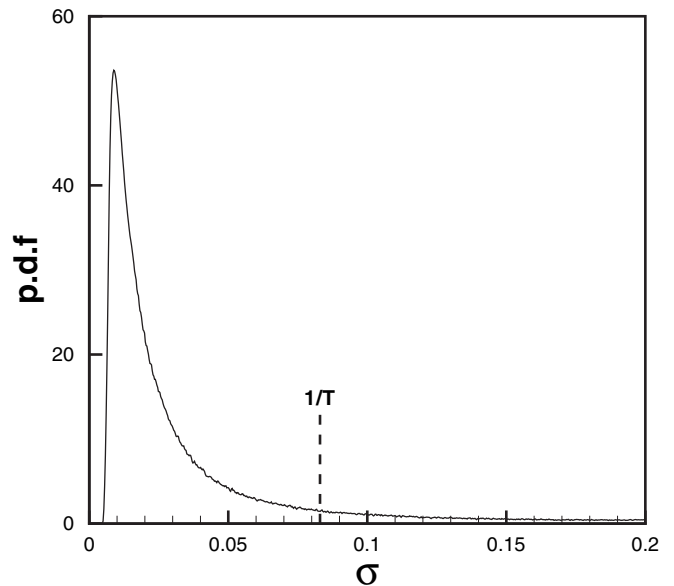

Fig. 7. P.d.f of strain rate computed on 60 501 Lagrangian trajectories in blinking vortex flow.
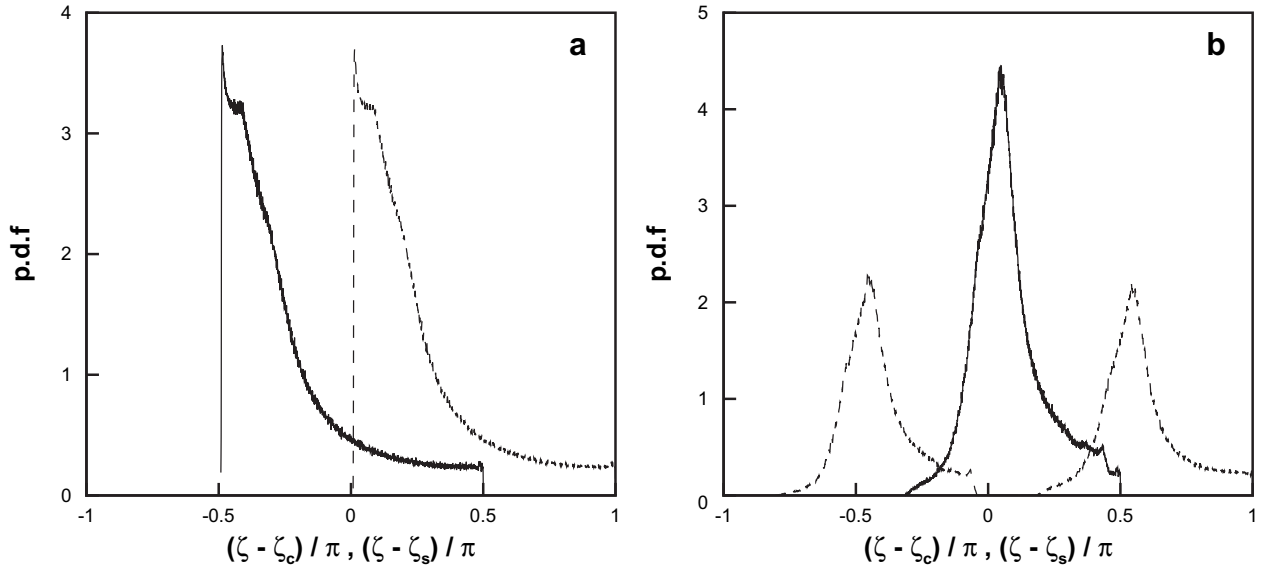
Fig. 8. P.d.f of tracer gradient alignment computed on 60 501 Lagrangian trajectories in blinking vortex flow; (a) $p(1)p(2)$ process; (b) $p(1)n(2)$ process; solid line: p.d.f of $(\zeta - \zeta_c)/\pi$; dashed line: p.d.f of $(\zeta - \zeta_s)/\pi$.
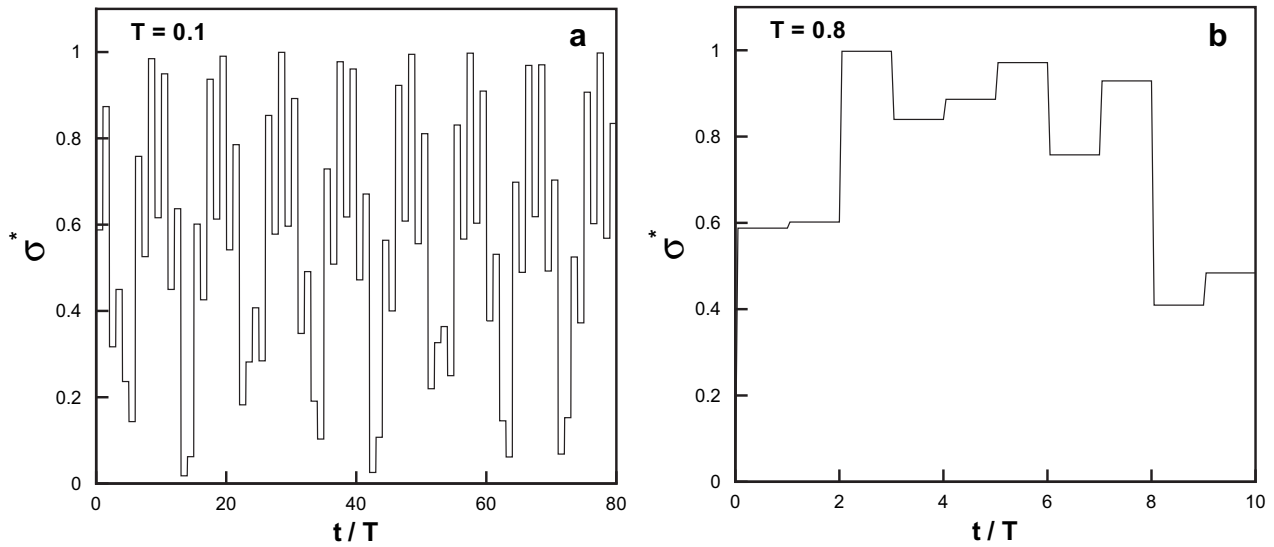

Fig. 9. Lagrangian evolution of strain rate for the test particle in sine flow; (a) $T = 0.1$; (b) $T = 0.8$.

It is this special behaviour which explains the difference in the local stirring properties of processes $p(1)p(2)$ and $p(1)n(2)$. This analysis is supported by statistics derived from the tracking of the 60 501 Lagrangian particles. As shown in Table 1, the mean strain rate is the same for both $p(1)p(2)$ and $p(1)n(2)$. However, the mean value of $\log|\mathbf{G}|$ is much larger at the end of the $p(1)n(2)$ process which indicates better local stirring. This difference is explained by the statistics of tracer gradient alignment; the gradient statistically tends to align closer to the compressional direction in the $p(1)n(2)$ process which, through the orientation term, $\sin \zeta$, brings about a larger norm growth rate, η^*.

3.2. Sine flow

As a second mixing system, we consider the sine flow [25] defined by the blinking of two nonlinear velocity fields, namely:

$$\mathbf{u}_0(x, y) = (\sin 2\pi y, 0); \mathbf{u}_1(x, y) = (0, \sin 2\pi x), \qquad (11)$$

which are alternately applied with half-period T. For both velocity fields, $\sigma_n = 0$. When velocity is given by $\mathbf{u}_0$:

$$\sigma_s = 2\pi \cos 2\pi y; \omega = -2\pi \cos 2\pi y, \qquad (12)$$

while when $\mathbf{u}_1$ is applied:

Table 1
Statistics computed on 60 501 Lagrangian trajectories for processes $p(1)p(2)$ and $p(1)n(2)$ of blinking vortex flow; $\langle . \rangle_{\text{final}}$ represents averaging over the 60 501 final values.

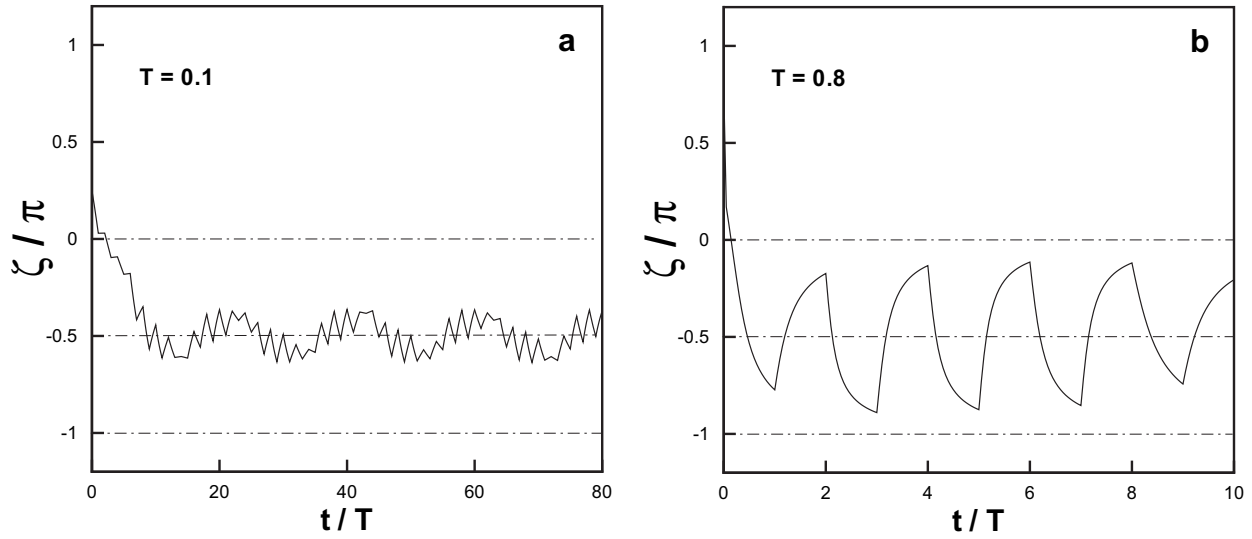| process	$\langle \sigma^* \rangle$	$\langle \log|\mathbf{G}| \rangle_{\text{final}}$	$\langle |\zeta - \zeta_c|/\pi \rangle$	$\langle -\sin\zeta \rangle$	$\langle \eta^* \rangle$
p(1)p(2)	0.16	0.96	0.31	0.51	0.052
p(1)n(2)	0.16	2.6	0.12	0.89	0.14

Fig. 10. Lagrangian evolution of tracer gradient orientation for the test particle in sine flow; (a) $T = 0.1$; (b) $T = 0.8$.
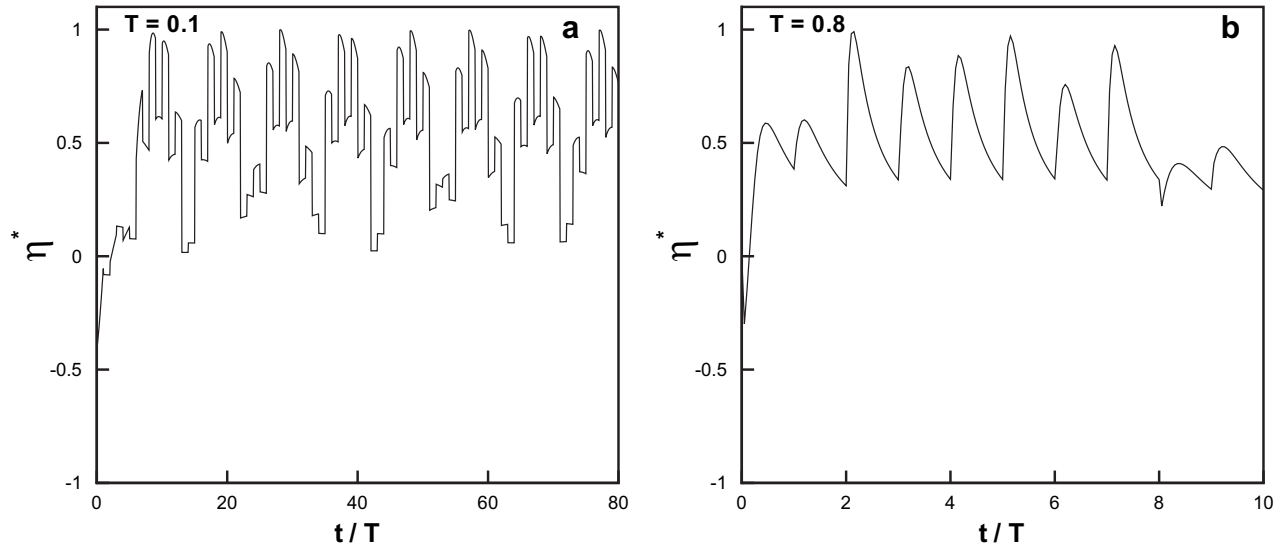

Fig. 11. Lagrangian evolution of tracer gradient norm growth rate for the test particle in sine flow; (a) $T = 0.1$; (b) $T = 0.8$.

$$\sigma_s = 2\pi \cos 2\pi x; \omega = 2\pi \cos 2\pi x. \qquad (13)$$

Moreover, in both cases $d\Phi/dt = 0$ and effective rotation is thus restricted to vorticity. The strain persistence parameter, then, is $r = \omega/\sigma$ which leads to $r = -1$ for $\boldsymbol{u}_0$ velocity field and $r = 1$ for $\boldsymbol{u}_1$. The protocol based on alternating $\boldsymbol{u}_0$ and $\boldsymbol{u}_1$ velocity fields thus comes to unsteady forcing through strain persistence which periodically takes values -1 and 1 all over the flow field.

As in the case of the blinking vortex flow, Eqs. (1) and (2) are solved along Lagrangian trajectories. The latter are integrated using velocity given by Eq. (11) and assuming periodic conditions on the boundaries of the computational domain. The protocol conditions are the same as those considered by Cortelezzi et al. [26]; the total duration of the process is $T_{tot} = 8$ and three different half-periods are examined, namely $T = 0.1$, $T = 0.4$ and $T = 0.8$.

The effect of period time, T, on the Lagrangian evolution of the tracer gradient is illustrated by tracking a test particle starting from coordinates $x(0) = 0$ and $y(0) = 0.15$; the initial orientation of the

gradient is $\zeta(0) = \pi/4$ and its initial norm is $|\boldsymbol{G}|(0) = 1$. Fig. 9 displays the strain rate history along the particle trajectory for $T = 0.1$ and $T = 0.8$ with $\sigma^* = \sigma/2\pi$. On an average, the strain rate experienced by the tracer gradient is larger in the latter case. However, through its action on gradient orientation, unsteady forcing resulting from the periodical variations of r has a significant influence on the growth rate of the gradient norm. As shown in Fig. 10, fast unsteady forcing – $T = 0.1$ – precludes alignment of the tracer gradient with directions given by either $r = 1$ ($\zeta_s = 0$) or $r = -1$ ($\zeta_s = -\pi$) and promotes alignment close to the compressional direction, $\zeta_c = -\pi/2$, corresponding to $\langle r \rangle = 0$. For $T = 0.8$, though, the tracer gradient rather reveals a tendency to align with directions defined by $r = \pm 1$. This difference in alignment results in a comparable norm growth rate, η^* – with $\eta^* = \eta/2\pi$ –, for $T = 0.8$ and $T = 0.1$ (Fig. 11), despite an overall lower strain rate in the latter case.

More general statistics are computed over the trajectories of 40 401 particles initially set on a regular mesh covering the spatial
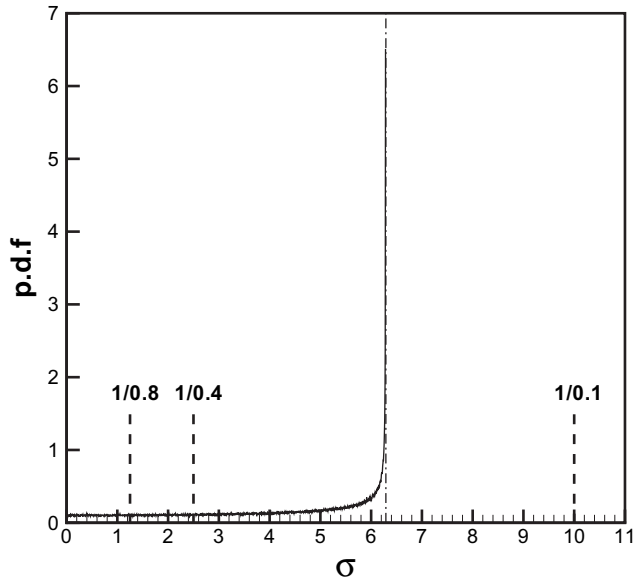
Fig. 12. P.d.f of strain rate computed on 40 401 Lagrangian trajectories in sine flow.

Table 2
Statistics computed on 40 401 Lagrangian trajectories in sine flow for $T = 0.1$, $T = 0.4$ and $T = 0.8$; $\langle . \rangle_{\text{final}}$ represents averaging over the 40 401 final values.

T	$\langle \sigma^* \rangle$	$\langle \log|\boldsymbol{G}| \rangle_{\text{final}}$	$\langle |\zeta - \zeta_{\text{c}}|/\pi \rangle$	$\langle -\sin\zeta \rangle$	$\langle \eta^* \rangle$
0.1	0.64	6.6	0.081	0.95	0.61
0.4	0.64	5.8	0.15	0.85	0.53
0.8	0.64	4.8	0.22	0.72	0.45

the blinking vortex flow, fast variations of strain persistence preclude alignment with equilibrium orientation, ζ_{s}. This alignment is much better for $T = 0.4$ and $T = 0.8$ than for $T = 0.1$. For the latter period time, the tracer gradient orientation does not keep up with strain persistence variations and remains close to the direction determined by mean strain persistence, $\langle r \rangle = 0$, namely, the local compressional direction, ζ_{c}.

As a result, the smaller the period time, the better the conditions for local stirring. Table 2 shows that the mean strain rate is the same for the three values of T. However, the growth rate of tracer gradient norm is improved as T is decreased. This is clearly due to better alignment with compressional direction which, through directional term, $\sin \zeta$, results in larger norm growth rate, η^*.

3.3. Distribution of stirring properties

Local growth rate of tracer gradient norm is relevant to local stirring – or stretching –, but diagnosis of the whole flow field needs the distribution of stirring properties over the domain. This question has already been discussed [27,28]. The non-dimensional integral $I_\eta(x_0, y_0) = \int_0^{T_{\text{tot}}} \eta(x_0, y_0; t) \mathrm{d}t$ – where T_{tot} is the total duration of the protocol – computed along Lagrangian trajectories and plotted in function of initial coordinates, (x_0, y_0), of each trajectory gives information about distribution of stirring properties [29].

Maps of $I_\eta(x_0, y_0)$ for the blinking vortex flow are shown in Fig. 14. In comparison to protocol $p(1)p(2)$, $p(1)n(2)$ ensures both large local growth rate of tracer gradient norm and chaotic conditions causing uniform distribution of stirring properties over a significant part of the domain. However, the latter ideal conditions are not always fulfilled. Chaotic regime in the sine flow, for instance, is reached for large enough period time, T [26]. As is clear
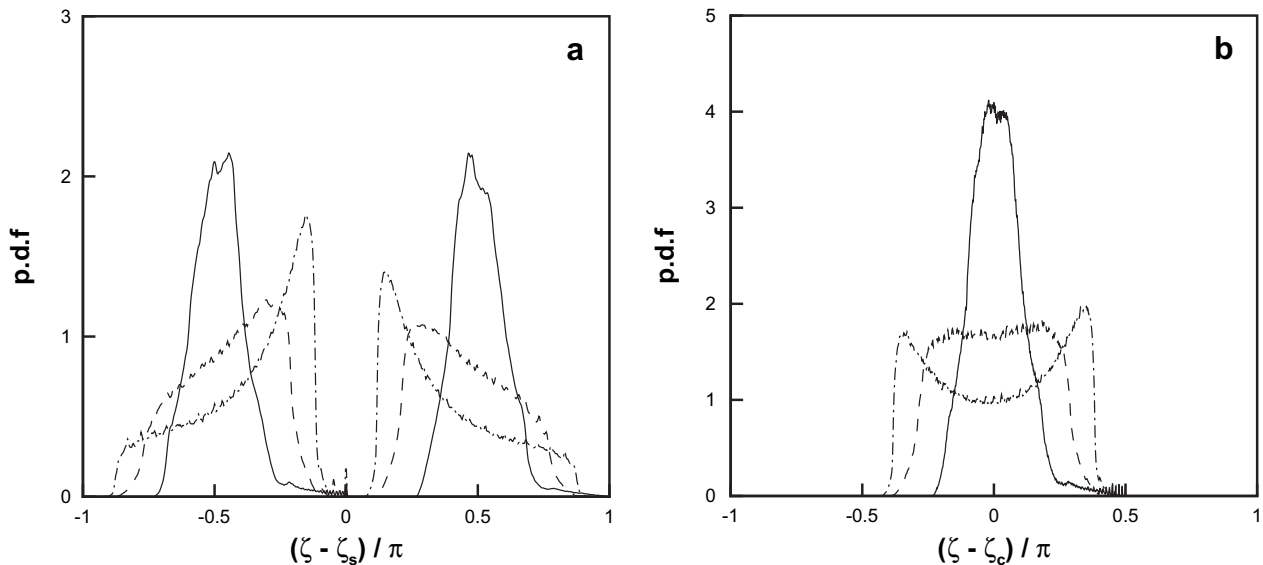
domain corresponding to $0 \leq x \leq 1$ and $0 \leq y \leq 1$. The initial norm of tracer gradient is unity and its initial orientation is $\zeta(0) = 0$. As in the blinking vortex flow, the gradient statistics weakly depend on initial orientation.

Fig. 12 shows the strain rate p.d.f computed over the set of Lagrangian trajectories. The p.d.f clearly peaks near the maximum strain rate, $\sigma_{\text{m}} = 2\pi$. In fact, as shown by Eqs. (11)–(13), maximum strain rate coincides with the minimum value of velocity; Lagrangian particles thus spend most of residence time in high-strain-rate regions. From Fig. 12, it is clear that for the smallest value of period time, $T = 0.1$, variations of strain persistence are too fast for the tracer gradient to respond. The larger period times, $T = 0.4$ and $T = 0.8$, by contrast, correspond to frequencies of strain persistence variations smaller than the most probable strain rate and must lead to better response of the tracer gradient. This is confirmed by orientation p.d.f's displayed in Fig. 13. As in the case of

Fig. 13. P.d.f of tracer gradient alignment computed on 40 401 Lagrangian trajectories in sine flow; (a) p.d.f of $(\zeta - \zeta_{\text{s}})/\pi$; (b) p.d.f of $(\zeta - \zeta_{\text{c}})/\pi$; solid line: $T = 0.1$; dashed line: $T = 0.4$; dashed-dotted line: $T = 0.8$.
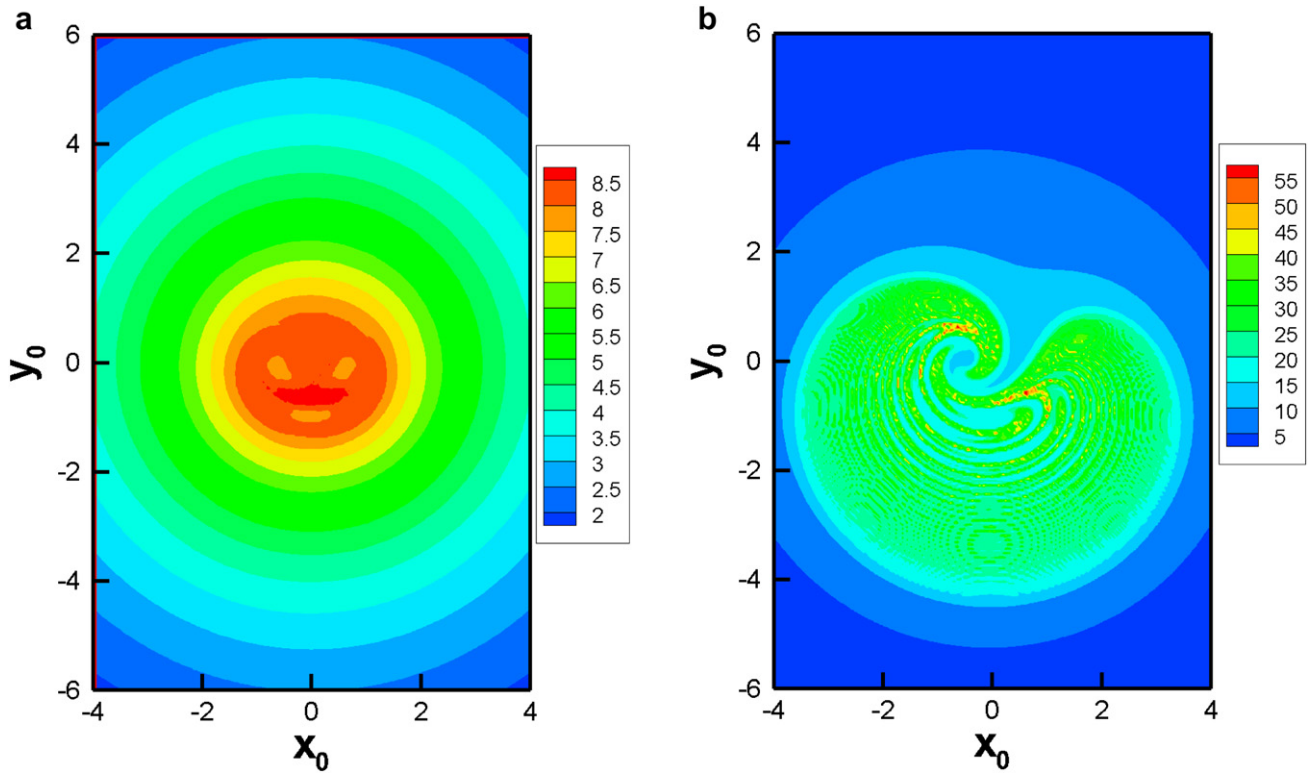
Fig. 14. Maps of $I_\eta(x_0, y_0)$ in blinking vortex flow; (a) $p(1)p(2)$ process; (b) $p(1)n(2)$ process.
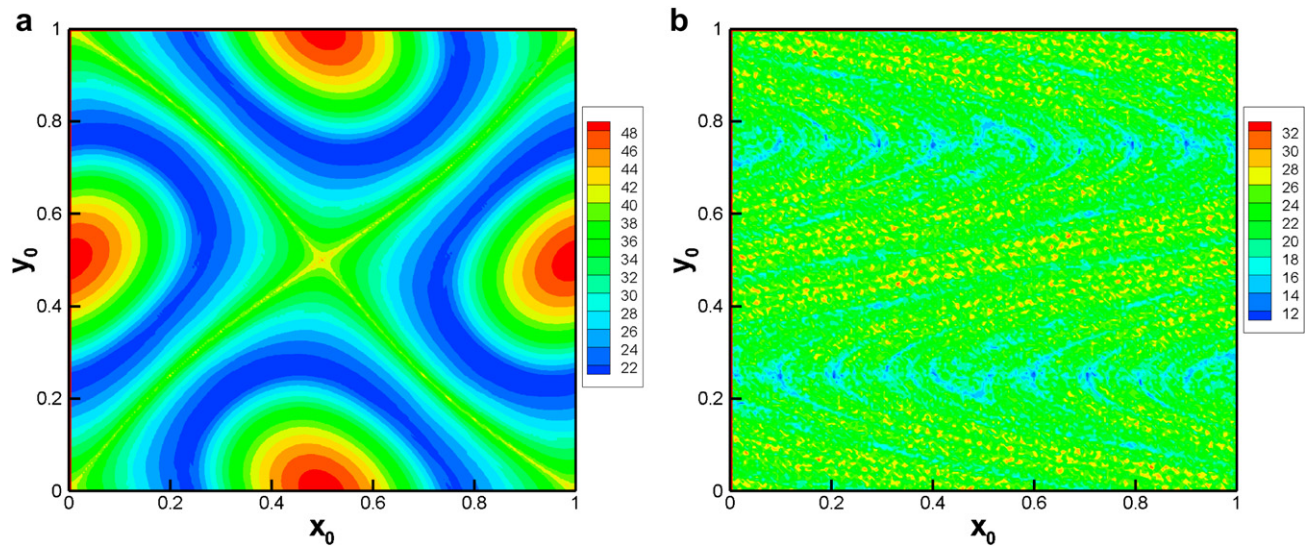

Fig. 15. Maps of $I_\eta(x_0, y_0)$ in sine flow; (a) $T = 0.1$; (b) $T = 0.8$.

from Fig. 15, a small value of T – rapid forcing –, then, does lead to significant increase of tracer gradient norm as explained in Section 3.2, but does not ensure that stirring properties are uniformly distributed. Interestingly, $I_\eta(x_0, y_0)$ fields coincide with Poincaré maps for the sine flow [26]. For the blinking vortex flow [23], they are symmetrical to Poincaré maps. Through the integrated norm growth rate they thus include information on both global mixing and stirring – or stretching – flow properties. Their close analogy with Poincaré maps confirms the above-mentioned connection (Section 1) between the tracer gradient properties and the structure of mixing patterns.

4. Conclusion

The behaviour of the gradient of a tracer has been investigated in two model flows which often serve to mimic mixing systems, namely, the blinking vortex flow and the sine flow. The velocity gradient tensor and related quantities indicating local stirring properties have been exactly derived from the analytical definition of each velocity field. In particular, in both flows the strain persistence parameter reveals a special behaviour. In the blinking vortex flow rotation of agitators in the same direction leads to a constant strain persistence – -1 or 1, depending on rotation direction –, while

alternating clockwise and counterclockwise rotation drives strain persistence to periodically take values -1 and 1. In the sine flow strain persistence also undergoes the latter periodical variations.

The numerical study has shown that: i) unsteady forcing resulting from strain persistence variations experienced along Lagrangian trajectories significantly affect the tracer gradient properties through local alignment. More specifically, strain persistence variations occuring on a time scale shorter than the response time scale of the tracer gradient drive the latter to stay aligned close to the direction – say, $\zeta_{\langle r \rangle}$ – defined by the averaged strain persistence. This shows that the dynamics of the tracer gradient already emphasized in the laminar Bénard – von Kármán street [16,17] is also observed in model mixing flows and is most likely not a feature peculiar to a given flow; ii) in both the blinking vortex and the sine flows local stirring properties are deeply influenced by unsteady forcing imposed by strain persistence variations. Indeed the special alternating behaviour of strain persistence caused by flow operation makes $\zeta_{\langle r \rangle}$ coincide with the local compressional strain direction which promotes increase of the tracer gradient and thus local stirring.

Work in progress is addressing more complex mixing flows in which forcing is caused by both time and space variations of strain persistence.

Acknowledgements

References

[1] H. Tennekes, J.L. Lumley, A First Course in Turbulence, eighth ed. The MIT Press, Cambridge (MA), 1982.
[2] S. Corrsin, J. Appl. Phys. 22 (1951) 469.
[3] S. Corrsin, AIChE J. 10 (1964) 870.
[4] J.M. Ottino, Annu. Rev. Fluid Mech. 22 (1990) 207.
[5] S. Wiggins, J.M. Ottino, Philos. Trans. R. Soc. Lond., Ser. A 362 (2004) 937.
[6] N. Nakamura, J. Atmos. Sci. 53 (1996) 1524.
[7] G. Lapeyre, P. Klein, B.L. Hua, Phys. Fluids 11 (1999) 3729.
[8] S. Goto, S. Kida, J. Fluid Mech. 586 (2007) 59.
[9] F. Városi, T.M. Antonsen Jr., E. Ott, Phys. Fluids 3 (1991) 1017.
[10] M.D. Finn, S.M. Cox, H.M. Byrne, J. Fluid Mech. 493 (2003) 345.
[11] G. Lapeyre, Chaos 12 (2002) 688.
[12] G. Brethouwer, J.C.R. Hunt, F.T.M. Nieuwstadt, J. Fluid Mech. 474 (2003) 193.
[13] A. Garcia, M. Gonzalez, Phys. Fluids 18 (2006) 058101.
[14] W.D. Smyth, J. Fluid Mech. 401 (1999) 209.
[15] G. Lapeyre, B.L. Hua, P. Klein, Phys. Fluids 13 (2001) 251.
[16] A. Garcia, M. Gonzalez, P. Paranthoën, Phys. Fluids 17 (2005) 117102.
[17] A. Garcia, M. Gonzalez, P. Paranthoën, Eur. J. Mech. B/Fluids 27 (2008) 433.
[18] A. Okubo, Deep-Sea Res. 17 (1970) 445.
[19] J. Weiss, Physica D 48 (1991) 273.
[20] E. Dresselhaus, M. Tabor, J. Fluid Mech. 236 (1992) 415.
[21] M. Tabor, I. Klapper, Chaos Solitons Fractals 4 (1994) 1031.
[22] H. Aref, J. Fluid Mech. 143 (1984) 1.
[23] E. Kin, T. Sakajo, Chaos 15 (2005) 023111.
[24] G. Lapeyre, Topologie du mélange dans un fluide turbulent géophysique, PhD thesis, Université Paris 6, 2000.
[25] M. Liu, F.J. Muzzio, R.L. Peskin, Chaos Solitons Fractals 4 (1994) 869.
[26] L. Cortelezzi, A. Adrover, M. Giona, J. Fluid Mech. 597 (2008) 199.
[27] G. Boffetta, G. Lacorata, G. Redaelli, A. Vulpiani, Physica D 159 (2001) 58.
[28] T.Y. Koh, B. Legras, Chaos 12 (2002) 382.
[29] G. Lapeyre, B.L. Hua, B. Legras, Chaos 11 (2000) 427.